Available online at www.sciencedirect.com
SCIENCE DIRECT
Journal of Power Sources 153 (2006) 130–135
JOURNAL OF POWER SOURCES
www.elsevier.com/locate/jpowsour

Short communication

Ultra large-scale simulation of polymer electrolyte fuel cells

Yun Wang, Chao-Yang Wang *

Electrochemical Engine Center (ECEC), and Department of Mechanical and Nuclear Engineering, The Pennsylvania State University, University Park, PA 16802, USA

Received 10 February 2005; accepted 5 March 2005
Available online 8 June 2005

Abstract

This paper reports on the computational performance and detailed results of ultra large-scale simulations of a 200 cm^2 polymer electrolyte fuel cell (PEFC) using a 23.5 million gridpoint mesh. The computer code is based on a comprehensive single-phase PEFC model that features a detailed membrane-electrode assembly (MEA) model, electron transport, thermal and species transport, coolant heat transfer, in addition to other standard functionalities. Two cases under dry operation are simulated and compared. One case concerns an infinitely large coolant flowrate and consequently a constant temperature of bipolar plates. The other case involves a finite flowrate and a lower inlet coolant temperature designed to avoid membrane dryout in the inlet region while alleviating electrode flooding in the outlet region.

Keywords: Computational fuel cell dynamics; Polymer electrolyte fuel cells; Large-scale simulation; Cooling

1. Introduction

Computer simulation of PEFCs has been an active research area: see the most recent comprehensive review of Wang [1]. Significant capabilities exist using the single-phase modeling approach. Notable examples include a detailed model of membrane-electrode assembly (MEA) [2–4], electron transport and direct prescription of constant current boundary condition [5,6], non-isothermal modeling and hence coupled consideration of water and thermal management [7], variable gas flow [8,9], transient analysis [10], and experimental validation against detailed current distribution data [11,12].

For single-phase calculations, Meng and Wang [13] first proposed a parallel computing methodology to handle large-scale simulations involving millions of gridpoints. They simulated a variety of wet-to-dry operating conditions with a five-channel serpentine flow-field and benchmarked the parallel computing performance to be greater than 7 × speed-up with 10 processors. The largest calculations reported so far were by Wang [1] (2.7 million cells); Shimpalee et al. [14] (5 million cells), and Wang and Wang [15] (2.7 million cells). However, the industry has a need for simulations using an order-of-magnitude larger mesh with reasonable computing time. This paper presents 23.5 million gridpoint calculations for the first time, herein termed ultra large-scale simulation to distinguish from prior studies of large-scale simulations. In addition, we will show a capability to perform co-simulation of electrochemical/transport phenomena in a PEFC and heat transfer in coolant channels. Such an integrated heat and water management tool is highly desirable in design and engineering of commercial-size PEFCs.

2. Numerical model

Fig. 1 shows the computational domain of the 200 cm^2 PEFC featuring a 24-channel, 3-pass serpentine flowfield, which includes the flow plates, gas and coolant channels, gas diffusion layers (GDLs), and catalyst layers on both the anode and cathode, as well as the membrane. The geometrical dimensions of various components in the cell are listed in Table 1.

* Corresponding author. Tel.: +1 814 863 4762; fax: +1 814 863 4848.
E-mail address: cxw31@psu.edu (C.-Y. Wang).

0378-7753/$ – see front matter © 2005 Elsevier B.V. All rights reserved.
doi:10.1016/j.jpowsour.2005.03.207

Nomenclature

c_p	specific heat ($J\,kg^{-1}\,K^{-1}$)
C_k	molar concentration of species k ($mol\,m^{-3}$)
D	mass diffusivity of species ($m^2\,s^{-1}$)
F	Faraday's constant (96,487 $C\,eq.^{-1}$)
I	current density ($A\,cm^{-2}$)
K	permeability (m^2)
P	pressure (Pa)
R	gas constant ($8.134\,J\,mol^{-1}\,K^{-1}$)
S	source term in transport equations
T	temperature (K)
$\vec{u}$	velocity vector ($m\,s^{-1}$)

Greek letters

α	net water transport coefficient per proton
ε	porosity
ϕ	phase potential (V)
κ	ionic conductivity ($S\,m^{-1}$)
λ	membrane water content, $\#H_2O/\#SO_3^-$
ρ	density ($kg\,m^{-3}$)
σ	electronic conductivity ($S\,cm^{-1}$)
τ	shear stress ($N\,m^{-2}$)
ξ	stoichiometric flow ratio

Superscripts and subscripts

a	anode
avg	average
c	cathode
e	electrolyte
eff	effective value
g	gas phase
k	species
m	membrane
s	electronic phase
sat	saturate value
w	water

2.1. Governing equations

The single-phase PEFC model employed in this work consists of nonlinear, coupled partial differential equations governing the conservation of mass, momentum, species, energy, and charge with electrochemical reactions. The equations can be written in the vector form, as [3–7]:

$$\text{Continuity equation}: \quad \nabla\cdot(\rho\vec{u}) = 0 \tag{1}$$

Momentum conservation :

$$\frac{1}{\varepsilon^2}\nabla\cdot(\rho\vec{u}\vec{u}) = -\nabla p + \nabla\cdot\tau + S_{\mathrm{u}} \tag{2}$$

$$\text{Species conservation}: \quad \nabla\cdot(\vec{u}C_k) = \nabla\cdot(D_k^{\mathrm{eff}}\nabla C_k) + S_k \tag{3}$$

$$\text{Energy conservation}: \quad \nabla\cdot(\rho c_p\vec{u}T) = \nabla\cdot(k^{\mathrm{eff}}\nabla T) + S_{\mathrm{T}} \tag{4}$$

$$\text{Proton transport equation}: \quad \nabla\cdot(\kappa^{\mathrm{eff}}\nabla\phi_{\mathrm{e}}) + S_{\phi_{\mathrm{e}}} = 0 \tag{5}$$

$$\text{Electron transport equation}: \quad \nabla\cdot(\sigma^{\mathrm{eff}}\nabla\phi_{\mathrm{s}}) + S_{\phi_{\mathrm{s}}} = 0 \tag{6}$$

where ρ, $\vec{u}$, p, C_k, T, ϕ_{e}, and ϕ_{s} denote the gas density, superficial fluid velocity vector, pressure, molar concentration of species k, temperature, electrolyte and electronic phase potentials, respectively. The species considered here are hydrogen, oxygen, and water. The various source terms, electrochemical properties, and thermophysical properties identified for various regions of a PEFC, as well as necessary boundary conditions, have been detailed in [3–7] and thus are not repeated here. Select physical properties most relevant to the present simulation results are listed in Table 1.

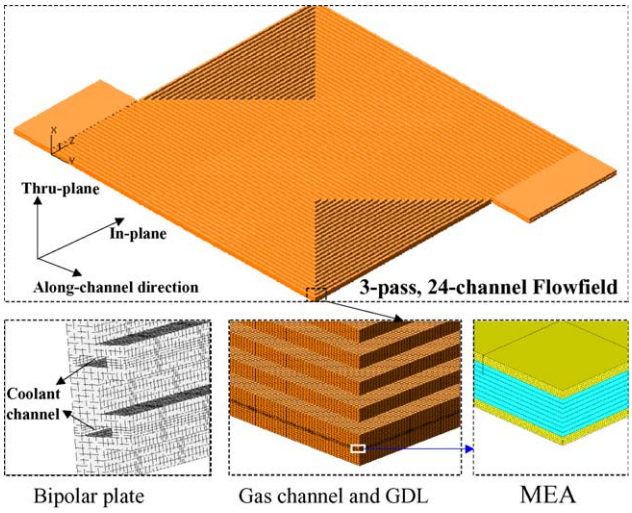

Fig. 1. Computational domain and mesh of a 200 cm^2 PEFC.

2.2. Numerical procedure

The conservation equations, Eqs. (1)–(6), are solved by the commercial package, Fluent®, with the SIMPLEC algorithm [16], using a parallel computational methodology for a Linux PC cluster. The SIMPLEC algorithm is to update the pressure and velocity fields from the solution of the pressure corrections equation, solved by algebraic multigrid (AMG) method [17]. Following the solution of the flow field, the energy, species, proton, and electron equations are solved. Approximately 23.5 million computational elements ($46\times900\times600$) are employed to capture details of flow, thermal, electrochemical and mass transport phenomena in the PEFC. The MEA, where the important electrochemical

Table 1
Geometrical and physical parameters [9,19]

Quantity	Value
Gas channel depth	1.0 mm
Gas channel width	1.0 mm
Land width	1.0 mm
Diffusion layer thickness	0.2 mm
Catalyst layer thickness	0.01 mm
Membrane thickness	0.045 mm
Fuel cell footprint area	143 mm × 143 mm
Anode/cathode/coolant flow	Co-flow
Anode/cathode pressure, P	2.0/2.0 atm
Average current density, I_{avg}	1.0 A cm^{-2}
Stoichiometric ratio ξ in the anode/cathode	2.0/2.0
RH of anode/cathode inlet @ 80 °C	50%/50%
GDL porosity, ε	0.6
Catalyst layer porosity, ε_g	0.4
Volume fraction of ionomer in catalyst layer, ε_m	0.26
GDL permeability, K	10^{-12} m^2
Specific heat, c_p, of coolant (de-ionized water)	4182 J kg^{-1} K^{-1}
Water activity, a	$a = \frac{C_w RT}{p^{sat}}$, where $\log_{10} p^{sat} = -2.1794 + 0.02953\,(T - 273.15) - 9.1837 \times 10^{-5}(T - 273.15)^2 + 1.4454 \times 10^{-7}(T - 273.15)^3$
Water content in membrane, λ	$\lambda = \begin{cases} 0.043 + 17.81a - 39.85a^2 + 36.0a^3 & \text{for } 0 < a \le 1 \\ 14 + 1.4(a-1) & \text{for } 1 \le a \le 3 \end{cases}$

reactions and water back-diffusion process occur, is accurately captured by placing five and eight gridpoints in the catalyst layer and the membrane, respectively, along the through-plane direction. Details of the computational mesh are shown in Fig. 1. A constant average current density of 1 A cm^{-2} is specified as an input parameter, allowing the local current density and electronic phase potential to be predicted to vary spatially according to local operating conditions [6]. A simulation using 23.5 million cells typically requires about 600 iterations with the global mass balance less than 1% and residuals of species equations less than 10^{-6}, and takes nearly 20 h on 32 nodes of 2.8 GHz Intel Pentium 4 CPU and 1.0 GB DDR RAM.

3. Results and discussion

A 200 cm^2 PEFC is considered with the inlet gases having relative humidity (RH) of 50% relative to 80 °C on both anode and cathode sides. Other common operating conditions are detailed in Table 1. Two simulation cases are presented in this work. Case 1 involves an infinitely large flow rate of the coolant, thus effectively keeping the flow plate temperature constant at 80 °C or 353.15 K. In contrast, Case 2 simulates a thermal management scheme to enhance cell performance in which the coolant temperature is selected at 72 °C at the inlet and its flowrate at 2.9×10^{-6} m s^{-1}. The lower inlet coolant temperature helps to increase the local gas RH near the inlet and hence better hydrates the membrane, whereas the small coolant flowrate is used to allow the coolant temperature to increase by ∼10 °C from the inlet to outlet so as to alleviate possible cathode flooding in the exit region, as well as to elevate the coolant exit temperature for better heat dissipation in the radiator. The resulting cell voltages predicted under the two cooling conditions are contrasted in Table 2. There is a 26 mV gain in cell voltage in Case 2 as compared with Case 1. In addition, detailed contours of the current density, membrane temperature, membrane water content, and membrane water crossover coefficient are presented below to illustrate the predictive capabilities of such an ultra large-scale simulation tool.

Fig. 2 shows the current density distribution in Case 1. It can be seen that the current density initially increases along the cathode flow, as can be explained by the ohmic control of cell performance. The dry anode and cathode gases result in dryout of the membrane in the inlet region, thereby increasing the local ionic resistance. As gases travel through the fuel cell, membrane hydration improves by product water and hence its ionic resistance decreases downstream and the current density increases.

Fig. 3 shows the temperature distribution in the membrane in Case 1. Despite that the current collecting lands maintain the constant temperature of 80 °C due to infinitely large coolant flowrate, there is ∼3 K temperature rise in the membrane due to the limited in-plane thermal resistance of GDL. In addition, the membrane temperature increases along the cathode flow, in accordance with the increasing current density.

Table 2
Coolant conditions and cell voltages

	Case 1	Case 2
Coolant flow rate	Infinite	2.9×10^{-6} m s^{-1}
Coolant inlet temperature	353.15 K (80 °C)	345.15 K (72 °C)
Predicted cell voltage	0.590 V	0.616 V

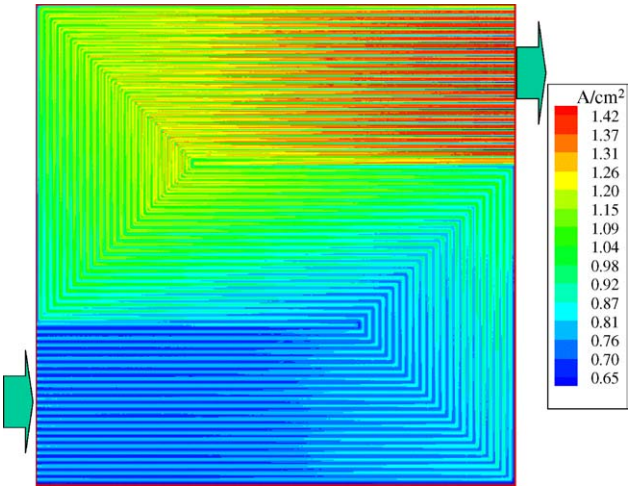

Fig. 2. Current density distribution in the membrane in Case 1.

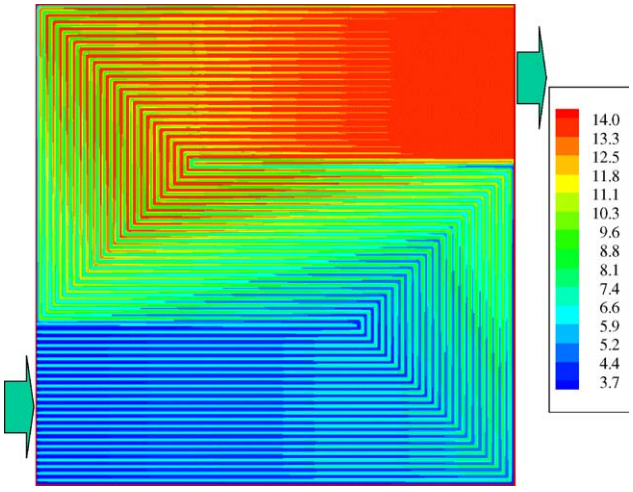

Fig. 4. Water content at the membrane–cathode interface in Case 1.

Fig. 4 presents the distribution of membrane water content at the interface between the membrane and cathode catalyst layer for Case 1. It can be seen that the cathode is dry in the inlet region in spite of water production. In addition, water content reaches the fully hydrated level, i.e. $\lambda = 14$, in the outlet region, resulting in likely occurrence of cathode flooding.

Fig. 4 points out two problems inherent in the design of Case 1. First, the dry gas feed, while preferred for the automotive application, causes membrane dryout in the inlet region. Secondly, the outlet gas stream is over-saturated. These two issues can be resolved by proper thermal control through the coolant flow design, such as in Case 2. Fig. 5 presents the temperature distribution in the cathode flow plate for Case 2. It is seen that this coolant design, using a lower inlet temperature and a small flowrate, creates a thermal gradient (345–355 K) from the inlet to the outlet regions. A significant benefit of this thermal gradient along the flow direction can be seen in Fig. 6, where membrane water content is displayed. As compared to Fig. 3 with isothermal cooling, Case 2 increases the membrane water content in the inlet region under lower local temperatures and at the same time maintains fully saturated gas in the outlet region under higher temperatures. The net result of this thermally graded fuel cell is that the membrane water content becomes more uniform.

As a result of the more uniform degree of membrane hydration, the current density near the inlet becomes higher, as shown in Fig. 7. In addition, more uniform current distribution results.

It is worth noting that the coolant condition in Case 2, however, results in greater temperature gradient in the membrane, as shown in Fig. 8. There is ∼12 K temperature difference between the inlet and outlet areas. This temperature non-uniformity could potentially cause membrane degradation due to thermal stresses [18].

Fig. 9 displays the net water transfer coefficient through the membrane, α, for Case 2. It can be seen that this coefficient, indicating water crossover through the membrane, varies spatially. In the inlet region of both anode and

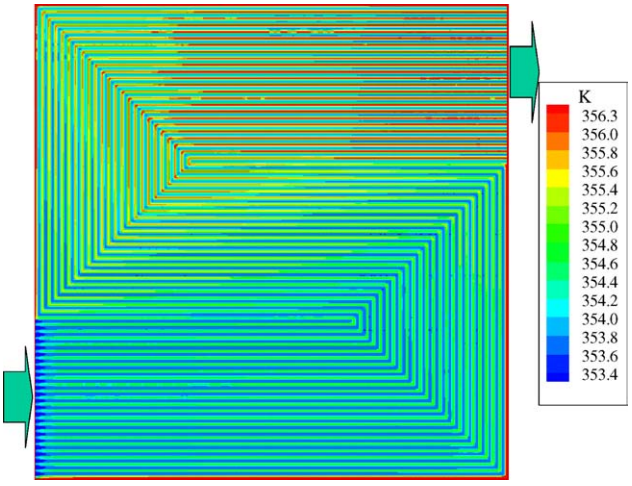

Fig. 3. Membrane temperature distribution in Case 1.

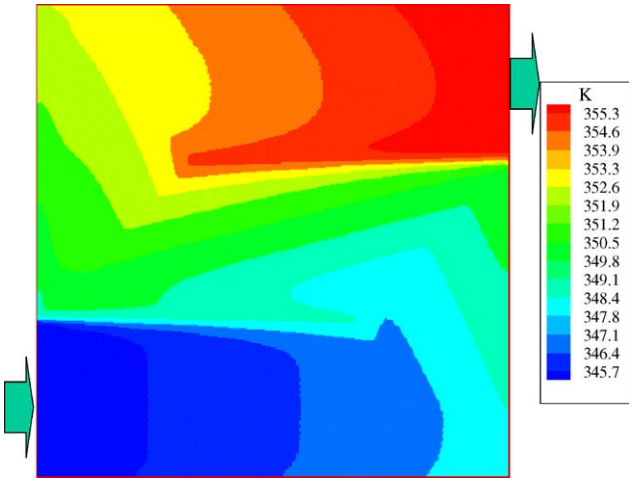

Fig. 5. Surface temperature at the cathode flow plate in Case 2.

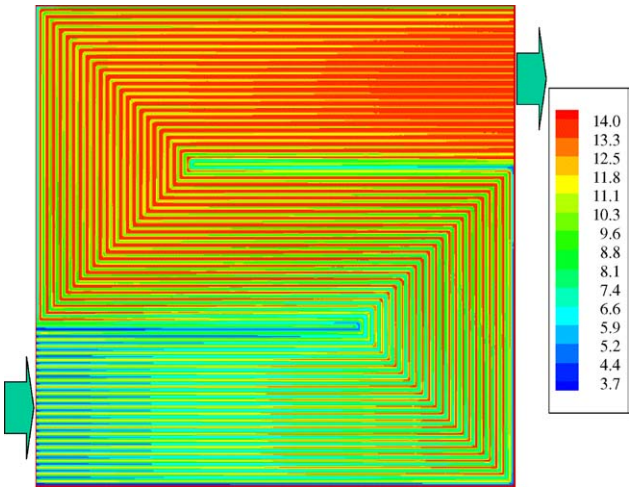

Fig. 6. Water content at the membrane–cathode interface in Case 2.

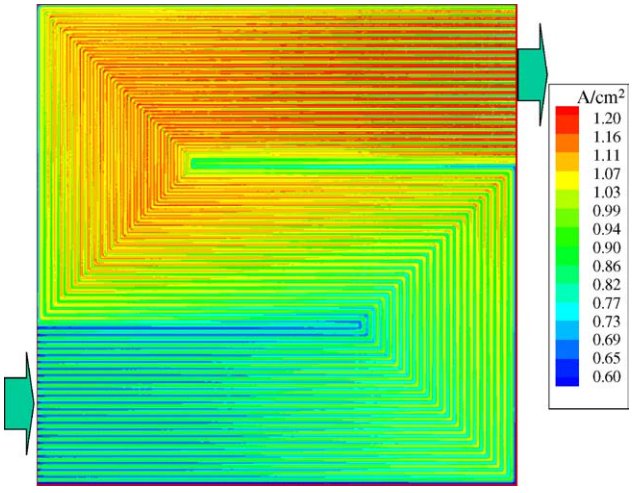

Fig. 7. Current density distribution in the membrane in Case 2.

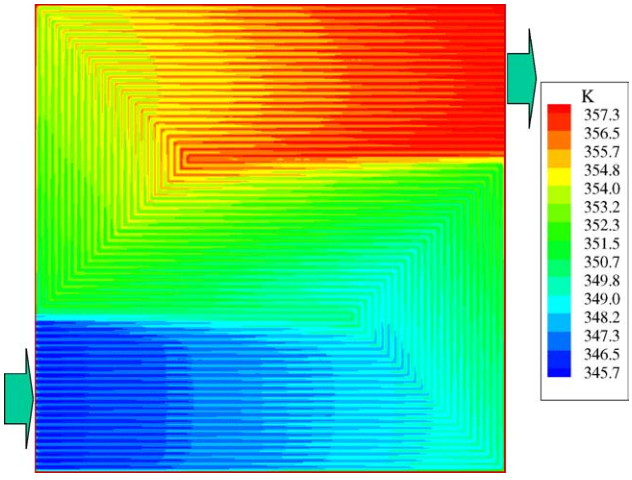

Fig. 8. Membrane temperature contours in Case 2.

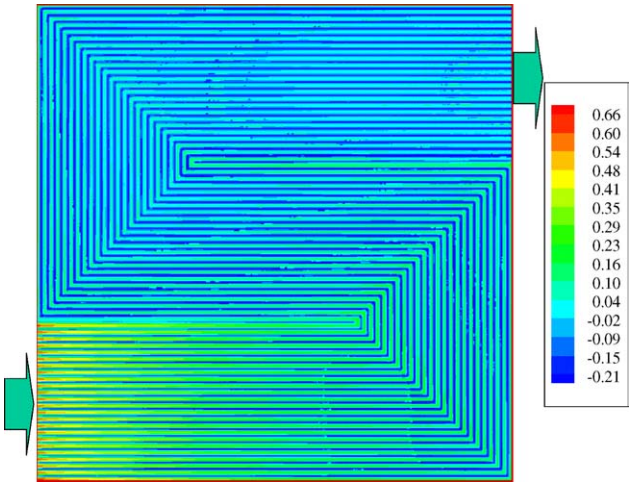

Fig. 9. Contours of net water transfer coefficient, α, across the membrane in Case 2.

cathode, the anode loses water to the cathode. Once the cathode gas gains moisture from product water, the net water flow is directed from the cathode to anode due to dominance of water back-diffusion.

4. Conclusions

Ultra large-scale simulations of a commercial-size PEFC with 24-channel 3-pass flowfield have been carried out to demonstrate the computational performance of a parallelized code for PEFCs, and to illustrate the internal phenomena and distributions of key parameters in a representative industrial cell as well as the profound coolant effects. Using a 32-processor PC cluster, we have shown a computing time of roughly 20 h for a simulation using a 23.5 million gridpoint mesh that considers comprehensive single-phase phenomena in a PEFC. In addition, the computed contours of current and water distributions indicate that low-humidity operation commonly used in automotive applications leads to membrane dryout in the inlet region and cathode flooding in the outlet region. These two seemingly conflicting issues can be simultaneously resolved by using a cooling scheme where a lower inlet coolant temperature and a small coolant flowrate are employed to create a thermal gradient along the cathode gas flow. The resulting “cold” inlet region maintains high relative humidity despite the dry gas supply, and the “hot” outlet region alleviates susceptibility of cathode flooding.

While the present paper exemplifies only one application of the ultra large-scale simulation tool, numerous other applications of the same computational intensity have been carried out routinely at this research laboratory as well as several automotive companies.

Acknowledgements

Support for this work by industrial sponsors of ECEC is gratefully acknowledged.

References

[1] C.Y. Wang, Chem. Rev. 104 (2004) 4727–4766.
[2] V. Garau, H. Liu, S. Kakac, AIChE J. 44 (1998) 2410–2422.
[3] S. Um, C.Y. Wang, K.S. Chen, J. Electrochem. Soc. 147 (2000) 4485–4493.
[4] S. Um, C.Y. Wang, J. Power Sources 125 (2004) 40–51.
[5] H. Meng, C.Y. Wang, J. Electrochem. Soc. 151 (2004) A358–A367.
[6] H. Meng, C.Y. Wang, Fuel Cells, in press.
[7] H. Ju, H. Meng, C.Y. Wang, Int. J. Heat Mass Transfer 48 (2005) 1303–1315.
[8] S. Dutta, S. Shimpalee, J.W. Van Zee, J. Appl. Electrochem. 30 (2000) 135–146.
[9] Y. Wang, C.Y. Wang, J. Electrochem. Soc. 152 (2005) A445–A453.
[10] Y. Wang, C.Y. Wang, Electrochim. Acta 50 (2005) 1307–1315.
[11] H. Ju, C.Y. Wang, J. Electrochem. Soc. 151 (2004) A1954–A1960.
[12] H. Ju, C.Y. Wang, S. Cleghorn, U. Beuscher, J. Electrochem. Soc., in press.
[13] H. Meng, C.Y. Wang, Chem. Eng. Sci. 104 (2004) 4727–4766.
[14] S. Shimpalee, S. Greenway, D. Spuckler, J.W. Van Zee, J. Power Sources 135 (2004) 79–87.
[15] Y. Wang, C.Y. Wang, J. Power Sources, in press.
[16] S.V. Patankar, Numerical Heat Transfer and Fluid Flow, Hemisphere Publishing Corp., New York, 1980.
[17] B.R. Hutchinson, G.D. Raithby, Numer. Heat Transfer 9 (1986) 511–537.
[18] D.P. Wilkison, J. St-Pierre, Durability, in: W. Vielstich, H. Gasteiger, A. Lamm (Eds.), Handbook of Fuel Cells: Fundamentals, Technology and Applications, vol. 3, John Wiley & Sons Ltd., 2003, p. 611.
[19] T.E. Springer, T.A. Zawodinski, S. Gottesfeld, J. Electrochem. Soc. 136 (1991) 2334–2341.